Vibrational correlation functions of hydrogen-terminated C(111)-(1×1) and Si(111)-(1×1) surfaces

B. Sandfort, A. Mazur, and J. Pollmann
Institut für Theoretische Physik II—Festkörperphysik, Universität Münster, D-48149 Münster, Germany
(Received 23 September 1994)

We report lattice-dynamical calculations of surface and subsurface displacement-correlation functions of hydrogen-terminated (111) surfaces of diamond and Si. These are evaluated employing a semiempirical total-energy scheme together with a 38-layer slab geometry. The total-energy scheme has recently been shown to yield a very accurate description of phonons at these surfaces in excellent agreement with available high-resolution electron-energy-loss spectroscopy data. The calculated vibrational correlation functions, such as mean-square displacements or mean-square relative displacements, to be reported in this paper show very pronounced orientational anisotropies and they are distinctly different on different layers at or near the surface. Even at the fourth layer, convergence to the respective bulk values is not yet reached. The significance of our results for an interpretation of surface-scattering experiments is assessed and it is shown that a fully quantitative interpretation of surface-scattering data cannot be achieved by using isotropic bulk displacement-correlation functions or the results of simple phenomenological models.

I. INTRODUCTION

Elastic or inelastic scattering of atoms, ions, electrons, or x-ray photons at surfaces is nowadays used in a routine fashion to experimentally determine the structure of clean and adsorbate-covered surfaces. Among the methods used are low-energy electron diffraction (LEED), ion channeling and blocking techniques like Rutherford backscattering (RBS), surface extended x-ray absorption fine structure (SEXAFS) measurements, or x-ray diffraction (XRD) and the x-ray standing-waves (XSW) method. The methods using x rays are distinguished by different sensitivities with respect to particular structural properties. The XSW method, for example, is particularly sensitive to adsorbate atoms with a high atomic number.[1] XRD is particularly sensitive to surfaces showing pronounced reconstructions[2] and SEXAFS measurements, finally, allow a very precise investigation of the atom positions in the near neighborhood of the x-ray-absorber atom.[3–6] To arrive at an analysis of the surface structure which is as complete as possible, very often these techniques are applied in combination. Since, for example, the XSW method allows one to determine adatom positions relative to the ideal bulk-lattice configuration, a complementary SEXAFS study can yield information on the substrate surface relaxation, in addition.[7,8] XRD measurements are successfully complemented by SEXAFS studies as well.[9] All scattering intensities are significantly influenced by the thermal vibrations of the target atoms and are therefore sensitively dependent on temperature. The thermal damping of LEED, XRD, and XSW or of SEXAFS data is governed by Debye-Waller or EXAFS Debye-Waller factors, respectively. Debye-Waller factors are defined in terms of displacement autocorrelation functions or mean-square displacements (MSD's) while EXAFS Debye-Waller factors involve displacement-correlation functions (DCF's) of different atoms as well. While MSD's can directly be measured nowadays (see Ref. 10, for example), the DCF's are not directly accessible and are therefore mostly taken from simple Debye models. For a fully quantitative analysis of surface-scattering data, respective thermal vibrational correlation functions for the atoms at or near the surface are thus a necessary prerequisite.

For the calculation of displacement-correlation functions the complete vibrational spectrum of the considered system must be known. The changed bonding configuration near a surface, as compared to the bulk, leads to a vibronic surface spectrum that can be significantly different from that of the underlying bulk crystal. Consequently, the MSD's and DCF's of atoms near the surface can be distinctly different from those of respective bulk atoms. Using isotropic bulk MSD's and DCF's or simple orientational Debye models for ideal surfaces thus may lead to an inappropriate consideration of the surface-specific dynamics in the interpretation of the data. Important effects such as, e.g., the anisotropy of the layer dependence of the MSD's, are ignored. This situation is very unsatisfactory, indeed. In particular, it has experimentally been shown by Martinez and coworkers,[10] e.g., for a Ga monolayer adsorbed at Si(111), that large anisotropies do in fact occur in surface MSD's. In this situation, only a quantitative calculation of the structure, the dynamics, and of vibrational correlation functions can procure a remedy.

Here we address the calculation of MSD's and DCF's for prototypical systems and demonstrate the surface sensitivity of these quantities in some detail. To this end, we have chosen the hydrogen-terminated Si(111)-(1×1) and C(111)-(1×1) surfaces, for which we have very recently reported the results of surface structure and surface phonon calculations.[11,12] These calculations were based on a semiempirical total-energy approach and slab geometries. The energy-optimized configurations show only small re-

0163-1829/95/51(11)/7168(8)/$06.00

laxations in both cases. For the hydrogen-terminated Si(111)-(1×1) surface[11] we have obtained surface phonon dispersions which are in excellent agreement with a whole body of high-resolution electron-energy-loss spectroscopy (HREELS) data.[13,14] For H:C(111)-(1×1) our results[12] are predictions, so far, since only very scarce experimental data are available for that system, to date. The MSD's and DCF's to be reported in this paper have been calculated using the eigenvalues and eigenvectors of the respective slab matrices for the optimally relaxed hydrogen-terminated surfaces from Refs. 11 and 12.

In this paper we report the calculation of displacement-correlation functions and mean-square displacements that have been obtained on equal footing from our lattice-dynamical investigations of H:Si(111)-(1×1) and H:C(111)-(1×1). The paper is organized as follows. In Sec. II we briefly summarize the definition and some basic properties of displacement-correlation functions. In Sec. III we address the thermal dependence of diffraction data. Here the key quantities are the mean-square displacements which are presented as a function of temperature for the two adsorption systems. In Sec. IV we address the temperature dependence of SEXAFS data for which both mean-square displacements and displacement-correlation functions are of paramount importance. A short summary concludes the paper in Sec. V.

II. DISPLACEMENT-CORRELATION FUNCTIONS

Within the harmonic approximation of lattice dynamics the equal-time displacement-displacement-correlation functions are defined as[15]

$$C_{\alpha\beta}(l\nu,l'\nu';T):=\langle u_\alpha(l,\nu)u_\beta(l',\nu')\rangle_T$$
$$=\frac{\hbar}{2N\sqrt{M_\nu M_{\nu'}}}\sum_{\lambda,\mathbf{k}}\frac{e_{\alpha\nu}(\lambda,\mathbf{k})e^*_{\beta\nu'}(\lambda,\mathbf{k})}{\omega(\lambda,\mathbf{k})}\coth\left[\frac{\hbar\omega(\lambda,\mathbf{k})}{2k_BT}\right]e^{i\mathbf{k}(\mathbf{R}^0_{l\nu}-\mathbf{R}^0_{l'\nu'})}. \quad (1)$$

The momentary position of basis atom ν with atomic mass M_ν in the lth unit cell is $\mathbf{R}_{l\nu}=\mathbf{R}^0_{l\nu}+\mathbf{u}(l,\nu)$. The equilibrium position of this atom is $\mathbf{R}^0_{l\nu}$ and its momentary displacement in the Cartesian direction α is $u_\alpha(l,\nu)$. The polarization vector and eigenfrequency of the λth vibrational mode with wave vector $\mathbf{k}$ in the first Brillouin zone are denoted by $\mathbf{e}(\lambda,\mathbf{k})$ and $\omega(\lambda,\mathbf{k})$, respectively. N is the number of unit cells in the macroscopic normalization volume, k_B is the Boltzmann constant, and T is the temperature. In the high-temperature limit, that is, if the thermal energy k_BT is much larger than the maximum vibrational frequency $\hbar\omega^{\max}:=\max\{\hbar\omega(\lambda,\mathbf{k})\}$, the DCF's obviously vary linearly with temperature. When displacement-autocorrelation functions or mean-square displacements $C_{\alpha\beta}(l\nu,l\nu;T)$ are considered, the phase factor in Eq. (1) simplifies to unity. Thus the MSD's for a given basis atom ν are obviously the same in all unit cells.

To calculate DCF's the complete vibrational eigenvalue spectrum $\{\omega(\lambda,\mathbf{k})\}$ and the complete set of polarization eigenvectors $\{\mathbf{e}(\lambda,\mathbf{k})\}$ for the considered system are needed. Consequently, the complete information on the specific surface dynamical properties enters the evaluation of vibrational correlation functions of surface systems.

For any given pair of atoms (l,ν) and (l',ν') the $C_{\alpha\beta}(l\nu,l'\nu';T)$ are the nine elements of a second rank tensor. They need not all be unequal to zero. This depends sensitively on the symmetry of the considered systems. We note in passing that the $\mathbf{C}$ tensor transforms exactly like the atomic force constant tensor.

III. MEAN-SQUARE DISPLACEMENTS

The influence of the thermal motion of atoms on diffraction amplitudes in elastic scattering is governed within the harmonic approximation by a Debye-Waller factor which is the second factor in the following thermodynamic expectation value:[15]

$$\langle e^{i\mathbf{k}\mathbf{R}_{l\nu}}\rangle_T=e^{i\mathbf{k}\mathbf{R}^0_{l\nu}}e^{-(1/2)\langle[\mathbf{k}\cdot\mathbf{u}(l,\nu)]^2\rangle_T}. \quad (2)$$

Here $\hbar\mathbf{k}$ is the momentum transfer from the scattered particle or wave to the lattice. The evaluation of the thermal expectation value in the Debye-Waller factor

$$\langle[\mathbf{k}\cdot\mathbf{u}(l,\nu)]^2\rangle_T=\sum_{\alpha,\beta}k_\alpha\langle u_\alpha(l,\nu)u_\beta(l,\nu)\rangle_Tk_\beta$$
$$=\sum_{\alpha,\beta}k_\alpha C_{\alpha\beta}(l\nu,l\nu;T)k_\beta \quad (3)$$

obviously involves mean-square displacements. For systems with a high symmetry, like diamond-structure bulk crystals, the MSD's are given by

$$C^b_{\alpha\beta}(T)=\tfrac{1}{3}\langle(\mathbf{u}^b)^2\rangle_T\delta_{\alpha\beta} \quad (4)$$

for all atoms in the crystal. The bulk $\mathbf{C}^b$ tensor is diagonal and its diagonal elements have the same value. The bulk MSD tensor is thus isotropic.

In a surface system, the MSD's depend on the layer m at which the considered basis atom μ resides and the $\mathbf{C}$ tensor needs no longer be diagonal. This means that the MSD's $C_{\alpha\beta}(m\mu,m\mu;T)$ at or near a surface can be anisotropic. For the clean, reconstructed Si(001)-(2×1) surface, e.g., we have shown previously[16] that two of the six nondiagonal elements of the MSD tensor are nonzero and that all three diagonal elements are different. The hydrogen-terminated C(111)-(1×1) or Si(111)-(1×1) surfaces have a higher symmetry. There is only one basis atom μ in the slab unit cell on each layer m. We can thus drop the index μ and characterize the MSD's by $C_{\alpha\beta}(m,m;T)$. For the C_{3v} symmetry of our systems all

nondiagonal elements of $C_{\alpha\beta}$ in the appropriate coordinate system vanish and only two different diagonal elements for each basis atom at or near the surface occur. The two surface-parallel MSD's on each layer m are identical and they differ from the surface-perpendicular component.

In the left panels of Figs. 1 and 2 we show the surface-perpendicular and the surface-parallel MSD's on the first four layers for H:Si(111)-(1×1) and H:C(111)-(1×1) as resulting from our calculations. The MSD's on a bulk layer are given for comparison, as well. Note the different scales in the left panels of these two figures. To highlight the specific surface influence on these surface MSD's and their respective deviations from the bulk MSD's we show in the right panels of Figs. 1 and 2 the corresponding *relative* mean-square displacements defined as $\langle [u_\alpha(m)]^2 \rangle_T / \langle (u_\alpha^b)^2 \rangle_T$. We recognize in both cases that the MSD's at the surface are strongly anisotropic and they are significantly larger than the respective bulk values. This is largely due to the reduced bonding of substrate atoms at or near the surface which allows an easier thermal motion of these atoms. It should be noted that even at the third substrate layer the MSD's still show pronounced anisotropies and they are still far away from their respective bulk values (see the right panels of Figs. 1 and 2, in particular). The extremely large MSD's for the H adatoms (see left top panels of Figs. 1 and 2) show very strong anisotropies and most noticeably the MSD's for surface-parallel thermal motions are much larger than those for the surface-perpendicular motions. In Table I we have listed the absolute and the relative root-mean-square (rms) displacement amplitudes of the atoms on the first four layers at room temperature for both adsorption systems. They are defined as $u_\alpha^{\rm rms}(m) = \sqrt{\langle [u_\alpha(m)]^2 \rangle_T}$ and $u_\alpha^{\rm rms}(m)/u_b^{\rm rms}$, respectively. Giant vibrational anisotropies of the adatoms and very large anisotropies for the substrate surface atoms are clearly to be recognized. There is no complete convergence to bulklike behavior even on the fourth atomic layer in both systems. The MSD's for H:Si(111)-(1×1) show a slower convergence to the bulk values than for H:C(111)-(1×1). This is related to the weaker bonding in Si as compared to diamond. As a matter of fact, the MSD's are converged within 1% to the respective bulk values for surface-parallel motions only at the eighth (sixth) and for surface-perpendicular vibrations only at the 15th (12th) layers, respectively, in the two adsorption

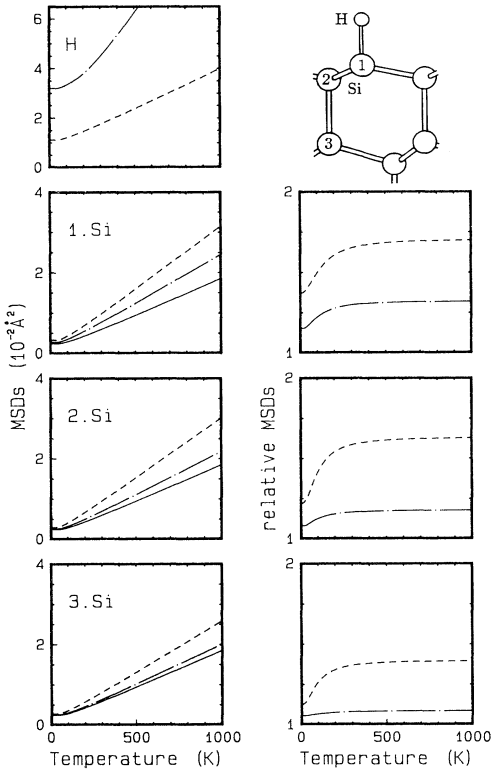

FIG. 1. Mean-square displacements (left panels) of the H adatom and of the Si atoms on the first three substrate layers [see the side view of the energy-optimized structure of the H:Si(111)-(1×1) surface given in the top right edge of this figure] as a function of temperature. The MSD's for the surface-perpendicular (— — —) and surface-parallel (—·—·—·) directions are compared in each case with the bulk MSD (——). The right panels show the corresponding relative MSD's for the surface-perpendicular (— — —) and surface-parallel (—·—·—·) directions. Note the difference in scale for the upper left panel.

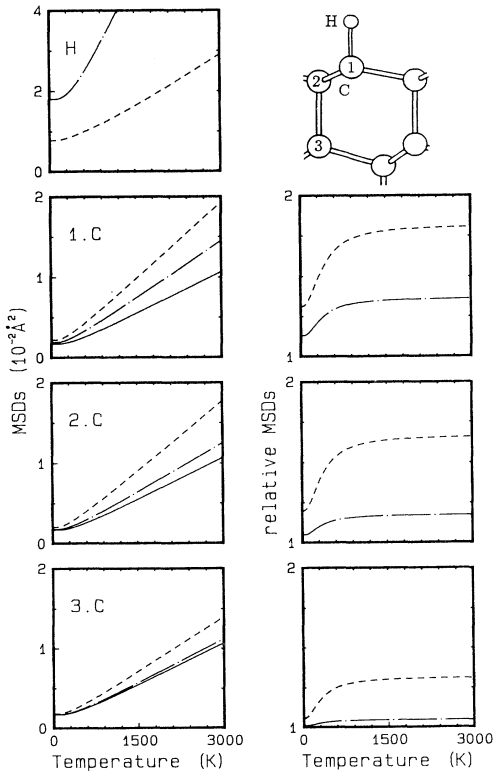

FIG. 2. Same as Fig. 1 but for H:C(111)-(1×1). Note the difference in scales between the left panels of Figs. 1 and 2, as well as that between the top left and the other three left panels in Fig. 2. Also the temperature scale is different from that of Fig. 1.

TABLE I. rms displacement amplitudes $u_\alpha^{\rm rms}$ (in Å) and relative rms displacement amplitudes $u_\alpha^{\rm rms}/u_b^{\rm rms}$ at $T=300$ K for an adsorbate layer atom (H), for substrate layer atoms (Si or C) on the first three layers of the respective substrates, and for a respective bulk atom.

	$u_\perp^{\rm rms}$	$u_\parallel^{\rm rms}$	$u_\perp^{\rm rms}/u_b^{\rm rms}$	$u_\parallel^{\rm rms}/u_b^{\rm rms}$
		H:Si(111)		
H	0.133	0.212	1.72	2.74
1.Si	0.099	0.088	1.29	1.14
2.Si	0.097	0.084	1.26	1.08
3.Si	0.091	0.080	1.17	1.04
Bulk	0.077	0.077	1.00	1.00
		H:C(111)		
H	0.092	0.139	2.09	3.17
1.C	0.053	0.048	1.22	1.10
2.C	0.051	0.046	1.17	1.05
3.C	0.047	0.044	1.08	1.01
Bulk	0.044	0.044	1.00	1.00

systems. At room temperature the rms amplitude normal to the surface is only 0.13 Å (0.09 Å) for H adsorbed at the Si (C) surface while the surface-parallel rms amplitude is 0.21 Å (0.14 Å) in the respective cases. For 800 K the respective values are 0.18 Å (0.11 Å) and 0.30 Å (0.17 Å). This peculiar behavior is due to the strong chemical bond between H and the respective substrate atoms which does not allow easy stretch-mode vibrations perpendicular to the surface (see Refs. 11 and 12 for that matter). On the other hand, easy bending-mode vibrations parallel to the surfaces do occur, giving rise to extremely large surface-parallel MSD's of the H adatoms. Thus in highly directional-bonded semiconductor adsorption systems surface-parallel MSD's of the surface layer atoms can be much larger than surface-perpendicular ones. The MSD's of the substrate layer atoms for perpendicular vibrations are larger than those for parallel vibrations. This behavior is of course related to the reduced bonding in the perpendicular direction that allows easier vibrational motions perpendicular than parallel to the surface. If a simple model description were used for all MSD's at these surfaces one would neglect their specific surface dynamical properties. The observed salient and unusual anisotropies in the MSD's at the surface should be taken into account when surface diffraction data are to be analyzed quantitatively.

Comparing the absolute MSD's in the left panels of Figs. 1 and 2 (note the difference in scales), one immediately recognizes that their values are considerably smaller for H:C(111)-(1×1) than for H:Si(111)-(1×1). In addition, the figures clearly reveal that the high-temperature or classical limit ($C_{\alpha\alpha}$ varies linearly with T) is reached in the case of the diamond surface at much higher temperatures than for the Si surface. The reason for this behavior lies in the fact that the bandwidth of the vibrational spectrum of diamond ($\hbar\omega^{\max}\cong 165$ meV) is much larger than that of Si ($\hbar\omega^{\max}\cong 65$ meV) and the energy of the H-C stretch mode (351 meV) is larger than that of the H-Si stretch mode (257 meV). See Refs. 11 and 12 for these energies. In the extreme quantum limit, i.e., at $T=0$ K the H adatoms show giant zero-point oscillations. In Table II we have listed the absolute and relative rms amplitudes at $T=0$ K for the adatoms, the first substrate surface layer atoms, and for bulk layer atoms of both adsorption systems. The adlayer atoms exhibit huge zero-point motions with relative rms amplitudes that are roughly two to four times larger than those of the substrate bulk atoms.

TABLE II. Analogous to Table I but at $T=0$ K. Note the huge zero-point rms amplitudes of the H adatoms, in particular, for surface-parallel displacements.

	$u_\perp^{\rm rms}$	$u_\parallel^{\rm rms}$	$u_\perp^{\rm rms}/u_b^{\rm rms}$	$u_\parallel^{\rm rms}/u_b^{\rm rms}$
		H:Si(111)		
H	0.105	0.178	2.18	3.71
1.Si	0.056	0.052	1.17	1.07
Bulk	0.048	0.048	1.00	1.00
		H:C(111)		
H	0.088	0.134	2.15	3.28
1.C	0.047	0.043	1.14	1.06
Bulk	0.041	0.041	1.00	1.00

It is very revealing to analyze the diagonal elements of the MSD tensor in the classical limit in some more detail. We note in Figs. 1 and 2 that the classical limit is essentially reached for the MSD's already considerably below the Debye temperatures of Si (645 K) and diamond (2230 K), respectively. Thus there seems to be a characteristic temperature for each MSD well below the Debye temperature which defines the onset of classical behavior of each $C_{\alpha\alpha}$, respectively. We arrive at the respective temperatures or frequencies by the following simple consideration. The classical or high-temperature limit of the MSD's follows from Eq. (1) as

$$C_{\alpha\alpha}(m,m;T)=\langle[u_\alpha(m)]^2\rangle_T=\frac{k_BT}{NM}\sum_{\lambda,\mathbf{k}}\frac{|e_{\alpha m}(\lambda,\mathbf{k})|^2}{\omega^2(\lambda,\mathbf{k})}\ . \tag{5}$$

On the other hand, we can consider the MSD of an atom at layer m in α direction as resulting from the thermal vibration of a one-dimensional oscillator of mass M and energy k_BT. This oscillator has a characteristic frequency $\Omega_\alpha(m)$ which depends both on the layer m considered and on the direction α of the oscillation. Its energy is $M\Omega_\alpha^2(m)\langle[u_\alpha(m)]^2\rangle_T$. Now this linear oscillation mode of an atom at a particular layer m in a particular direction α originates from a superposition of all the eigenmodes of the slab as is obvious from Eq. (5) because the complete sets of eigenvalues and eigenvectors of the dynamical matrix of the slab enter. But we can simply define effective frequencies of the respective one-dimensional oscillators for each set of α and m, which no longer depend on λ and $\mathbf{k}$. They are defined by

$$C_{\alpha\alpha}(m,m;T)=\langle[u_\alpha(m)]^2\rangle_T=:\frac{k_BT}{M\Omega_\alpha^2(m)}\ . \tag{6}$$

Evaluating $C_{\alpha\alpha}$ according to Eq. (5) then yields the characteristic frequencies or temperatures we have been looking for. We have listed the resulting energies $\hbar\Omega_\alpha(m)$ for both adsorption systems together with the

TABLE III. Effective energies $\hbar\Omega_\alpha(m)$ and temperatures $\Theta_\alpha(m)$ that characterize the onset of classical behavior of particular MSD's. (For the definition, see text.) They are to be compared to the Debye temperatures of 645 and 2230 K for Si and diamond, respectively, and to the temperatures that can be defined by equating the H-Si and H-C stretch-mode energies at the two surfaces to $k_B\Theta$. These temperatures are $\Theta_{H-Si}=2400$ K and $\Theta_{H-C}=4600$ K for the two systems, respectively.

	$\hbar\Omega_\alpha(m)$ (meV)		$\Theta_\alpha(m)$ (K)	
	$\alpha=\perp$	$\alpha=\parallel$	$\alpha=\perp$	$\alpha=\parallel$
		H:Si(111)		
H	99.3	57.3	1153	665
1.Si	20.2	23.0	235	267
2.Si	20.6	24.3	240	283
3.Si	22.3	25.4	259	295
Bulk Si	26.4	26.4	306	306
		H:C(111)		
H	197.1	108.3	2289	1257
1.C	68.5	79.0	796	917
2.C	71.5	85.1	830	988
3.C	80.5	90.0	934	1046
Bulk C	92.2	92.2	1071	1071

corresponding characteristic temperatures $\Theta_\alpha(m)$ in Table III. As expected they depend on the particular layer m considered and on the direction α of the oscillation parallel or perpendicular to the surface. The related temperatures for the mean-square displacements of the Si or C atoms are much smaller than the respective bulk Debye temperatures. Those for the MSD's of the H adatoms are smaller than characteristic temperatures which one can define corresponding to the H-substrate-atom stretch-mode energies (see the caption of Table III). Actually they all have roughly half the respective values. The largest effective frequencies, energies, or temperatures result for the oscillations of the H adatoms, in particular, for the perpendicular motion. Again, this is due to the large H-substrate-atom stretch-mode frequencies. From these results we infer, that it is not the bulk Debye temperature but the above-defined effective temperature which governs the onset of classical behavior of particular MSD's. The table again nicely reveals that the surface-parallel MSD's of the substrates converge faster to the respective bulk values than the surface-perpendicular quantities (see Table I for comparison).

IV. EXAFS DEBYE-WALLER FACTORS

Fine structures in extended x-ray absorption spectra result from an interference between the primary electron wave that is excited by an x-ray photon from the absorber atom and secondary waves which result from backscattering of the primary wave at the neighbors of the absorber atom (see Ref. 17, for example). The wavelength of the primary electron wave is uniquely determined by the energy of the x-ray photon and the binding energy of the electron in the crystal. The interference of primary and secondary waves varies between constructive and destructive depending on the energy of the absorbed x-ray photon. The absorption fine structure at the x-ray edges (EXAFS) thus allows one to obtain quantitative information on distances between the absorber atom and its neighbors. Since the involved atoms are all in thermal motion, their *relative thermal displacements* play a key role in the analysis of the spectra. The theory of EXAFS has been worked out in great detail by Sayers, Stern, and Lytle.[17,18] The oscillatory part of the absorption coefficient normalized to the structureless background is given as[3,17–19]

$$\chi(k)=\sum_n F(n,k)\sin[2kR(n)+\psi_n(k)]e^{-2k^2\sigma_n^2}, \tag{7}$$

with

$$\sigma_n^2:=\langle[\hat{\mathbf{R}}^0(n)\cdot(\mathbf{u}_n-\mathbf{u}_0)]^2\rangle_T . \tag{8}$$

Here $R(n)$ is the momentary distance between the absorber atom and a backscattering atom in the nth-neighbor shell and $R^0(n)$ is the respective equilibrium distance of these atoms. $\hat{\mathbf{R}}^0(n)$ is the unit vector $\mathbf{R}^0(n)/R^0(n)$ along the connection line between absorber and backscattering atom. The kinetic energy of the excited electron is $\hbar^2k^2/2m$. The total phase function is labeled $\psi_n(k)$ and $F(n,k)$ describes additional details of the scattering process (see, e.g., Ref. 3). The temperature-dependent damping of EXAFS spectra is determined by the exponential factor in Eq. (7) as has been shown by Beni and Platzman.[19] The latter depends on the kinetic energy of the excited electron and on the quantities σ_n^2. Obviously, these contain the projection of the relative thermal displacement $\mathbf{u}_n-\mathbf{u}_0$ of the two atoms onto the axis defined by their equilibrium positions. Consequently, Beni and Platzman[19] referred to σ_n^2 as mean-square relative displacement (MSRD). If we write down the MSRD explicitly as

$$\sigma_n^2=\langle[\hat{\mathbf{R}}^0(n)\cdot\mathbf{u}_n]^2\rangle_T+\langle[\hat{\mathbf{R}}^0(n)\cdot\mathbf{u}_0]^2\rangle_T -2\langle[\hat{\mathbf{R}}^0(n)\cdot\mathbf{u}_n][\hat{\mathbf{R}}^0(n)\cdot\mathbf{u}_0]\rangle_T \tag{9}$$

and make use of the fact that the vector $\hat{\mathbf{R}}^0(n)$ does not depend on temperature, we may write the MSRD as

$$\sigma_n^2=\sum_{\alpha\beta}R_\alpha^0(n)\{\langle u_\alpha(n)u_\beta(n)\rangle_T+\langle u_a(0)u_\beta(0)\rangle_T -2\langle u_a(n)u_\beta(0)\rangle_T\}R_\beta^0(n) . \tag{10}$$

Using Eq. (1) this can be rewritten as

$$\sigma_n^2=\sum_{\alpha\beta}R_\alpha^0(n)\{C_{\alpha\beta}(n,n;T)+C_{\alpha\beta}(0,0;T) -2C_{\alpha\beta}(n,0;T)\}R_\beta^0(n) . \tag{11}$$

Thus the MSRD is obviously a quadratic form and it is determined by the elements of the MSD tensors of the absorber atom and its neighbor in the nth-neighbor shell and by the DCF tensor of these two atoms. For a quantitative interpretation of EXAFS or SEXAFS spectra one thus needs, in principle, both the MSD's and the DCF's. Since these quantities are not known for many systems,

very often respective bulk values or so-called hybrid-schemes[19] have been employed in the interpretation in which measured MSD's and phenomenological DCF's calculated within an orientational Debye model are used. This approach has been employed, e.g., by McGrath and co-workers,[20,21] who investigated a whole variety of Si adsorption systems in great detail. We note in passing that for a metal adsorption system, namely, Co on Cu(111), the anisotropy of surface MSRD's have been investigated in a joint theoretical and experimental study.[22]

We have calculated MSRD's for the hydrogen-terminated Si(111)-(1×1) and C(111)-(1×1) surfaces from lattice dynamics. In these calculations both the MSD's and DCF's are evaluated microscopically on equal footing. We have chosen as absorber atom a substrate atom on the first substrate surface layer (Si or C, respectively) and have considered as backscatterers two different atoms on each of the first three neighboring shells as shown in Fig. 3. Our results for H:Si(111)-(1×1) and H:C(111)-(1×1) are shown in the left panels of Figs. 4 and 5, respectively. To highlight the influence of surface-induced anisotropies and of the DCF's on the MSRD's, we have defined *relative* MSRD's as

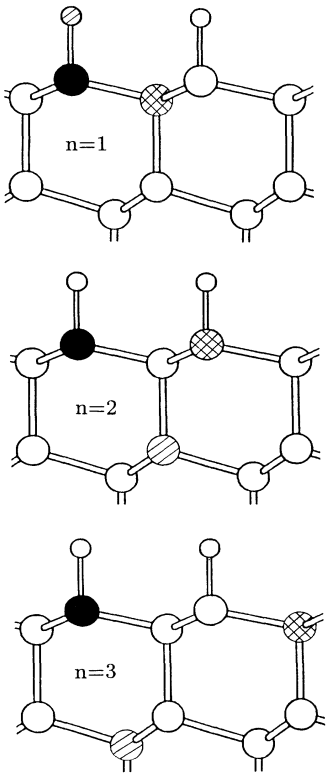

FIG. 3. Side views of the structure of the adsorption systems for which the MSRD's in Figs. 4 and 5 are shown. The absorber atom in the substrate surface layer is shown as a solid dot in each case. The two backscatterers considered for each shell are shown on the first- ($n=1$), second- ($n=2$), and third- ($n=3$) neighbor shells by hatched and cross-hatched circles, respectively.

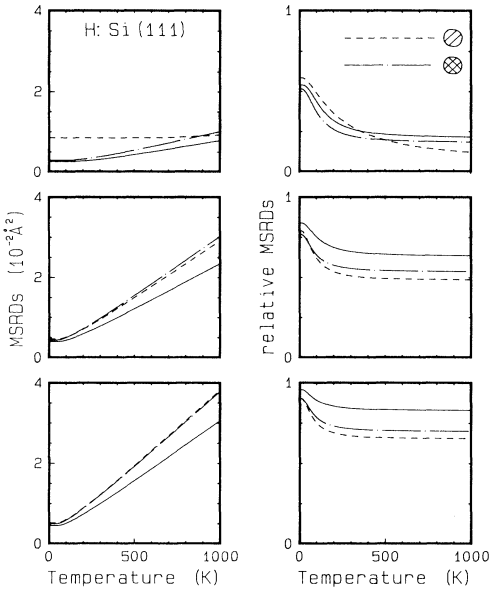

FIG. 4. Mean-square relative displacements σ_n^2 (left panels) and relative MSRD's $\sigma_n^2/\sigma_\infty^2$ (right panels) for H:Si(111)-(1×1). They are shown for two backscatterers on the first- ($n=1$), second- ($n=2$), or third- ($n=3$) neighbor shell of the absorber atom. The backscatterers considered are indicated in Fig. 3 for each case. The MSRD's and relative MSRD's shown by dashed lines (— — —) correspond to the hatched backscatterers in Fig. 3 and those shown by dashed-dotted lines (—·—·—·) correspond to the cross-hatched backscatterers in Fig. 3. For comparison we give the respective bulk curves that result when bulk MSD's and DCF's are used in the evaluation of the MSRD's.

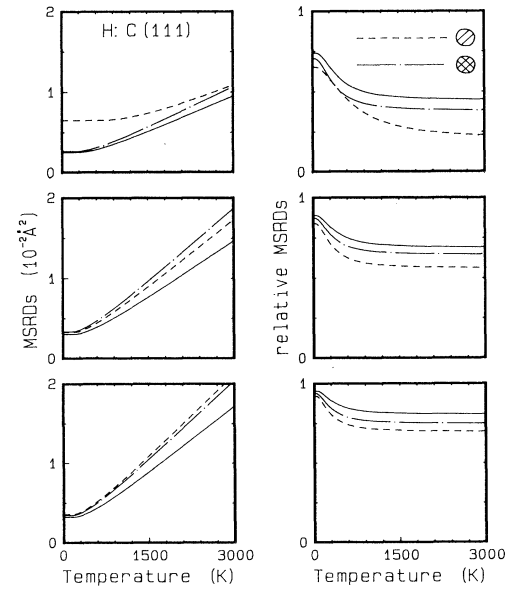

FIG. 5. Same as Fig. 4 but for H:C(111)-(1×1). Note the different scales.

$$\frac{\sigma_n^2}{\sigma_\infty^2}=\sigma_n^2\{\langle[\hat{\mathbf{R}}^0(n)\cdot\mathbf{u}_n]^2\rangle_T+\langle[\hat{\mathbf{R}}^0(n)\cdot\mathbf{u}_0]^2\rangle_T\}^{-1}\ . \quad (12)$$

Both the MSRD's and the relative MSRD's in Figs. 4 and 5 are shown for two different backscatterers in each neighbor shell $n=1$, 2, and 3. These are highlighted in the side views of the lattice in Fig. 3 by hatchings and cross-hatchings, respectively. In addition we have included in each panel the respective functions that result when bulk MSD's and bulk DCF's are employed in the evaluation. In that case σ_n^2 is of course the same for every backscatterer in an nth-neighbor shell. First we note that all MSRD's increase with temperature. Thus the fine structure in x-ray absorption spectra is increasingly damped with increasing temperature, as was to be expected. Second, we observe that the MSRD's on the first-neighbor shell are much smaller than those on the following shells. Thus the contributions of the nearest neighbors of the absorber atom to the EXAFS spectra are much less strongly damped than those of more distant neighbors. That is why EXAFS preferentially samples the short-range order giving structural information about the local surrounding of the absorber atom. Comparing the MSRD's for different neighbors on the same nth-neighbor shell, we see that only very weak anisotropies occur for $n\geq 2$. In these cases the backscatterers are all Si or C atoms, respectively. Since the hydrogen-terminated Si(111) and C(111) surfaces have almost the ideal bulk-lattice configuration, this result can easily be rationalized. When the first-neighbor shell of backscatterers is considered, there occur in both cases large anisotropies in σ_1^2 when H or Si(C) is considered as backscatterer (see top panels in Figs. 4 and 5). Similar anisotropies in σ_1^2 have been observed for Co adatoms and Cu(111) substrate surface atoms as backscatterers in Ref. 22. In particular, the MSRD for the H backscatterer on the first-neighbor shell at H:Si(111)-(1×1) shows only an extremely weak temperature dependence. Comparing the actual surface MSRD's with those that result when bulk MSD's and DCF's are employed, we see that the surface MSRD's are always larger. This corresponds to the behavior of the surface MSD's in Figs. 1 and 2 which are always larger than the bulk MSD's. Using bulk values for MSD's and DCF's in the calculation of MSRD's can thus lead to a k-dependent underestimate of the thermal damping of the fine structure in EXAFS spectra.

Considering the temperature dependence of the MSRD's in more detail, we note that they are linear in T in the high-temperature or classical limit. This was to be expected since the MSD's and DCF's are linear in T in this limit, as well, as we have pointed out in Sec. II. In the case of H:Si(111)-(1×1) we observe a linear T dependence of the MSRD's roughly above 300 K and for H:C(111)-(1×1) roughly above 900 K as can clearly be seen in the right panels of Figs. 4 and 5. When the H backscatterer in the first-neighbor shell is considered (see Fig. 3 and the top right panels of Figs. 4 and 5) classical behavior is reached only at much higher temperatures. This fully corresponds to the behavior of the respective MSD's in Figs. 1 and 2 and is again related to the strong H-substrate-atom bonds. The onset of classical behavior in Figs. 4 and 5 again nicely corresponds to the effective temperatures derived in Sec. III (see Table III). It is interesting to note that the slope of σ_n^2 increases with T for increasing neighbor order n. This is due to the fact that with increasing n the values of the DCF's, which reduce the values of the MSRD's, decrease and their influence on σ_n^2 vanishes. For very large n, the MSRD's are entirely determined by the MSD's of the absorber and the backscatterer in the nth-neighbor shell [see Eq. (11) for that matter]. For the same reason, the corresponding relative MSRD's approach unity in this limit. The limit $n\rightarrow\infty$ is obviously not yet reached by far on the third-neighbor shells (see right bottom panels in Figs. 4 and 5).

Considering the relative MSRD's in the quantum-mechanical limit for low temperatures, we note that they decrease with increasing temperature from their respective maxima at $T=0$ K. This simply means that the DCF's increase more strongly with T in this regime than the MSD's.

Finally we would like to emphasize that the MSRD's for H:Si(111)-(1×1) in Fig. 4 are roughly twice as large as those for H:C(111)-(1×1) in Fig. 5 (note the different scales). Again this is related to the stronger C-C and H-C bonds in the latter system as compared to the strengths of the Si-Si and Si-H bonds in the former. The relative MSRD's of both systems show almost quantitative correspondence for obvious reasons.

V. SUMMARY

We have presented displacement-correlation functions for the H:Si(111)-(1×1) and H:C(111)-(1×1) adsorption systems. In particular, MSD's and MSRD's were shown and discussed. The MSD's for atoms at and near the surfaces show very pronounced anisotropies in the surface-parallel and -perpendicular components. Most noticeably, the MSD's of the H adatoms are very large and they exhibit giant anisotropies. Due to their specific adatom-bonding configurations the surface-parallel MSD's are much larger than the surface-perpendicular MSD's in complete contrast to simple model expectations for the behavior of atoms at a surface. The MSRD's clearly show why surface EXAFS is very sensitive to the short-range order. For different backscatterers in the same neighbor shell the MSRD's show only weak anisotropies except for the case of the first-neighbor shell where both H and substrate atoms act as backscatterers. Figures 4 and 5 clearly show that MSRD's calculated with bulk MSD's and bulk DCF's are not appropriate at a surface. The pronounced differences in the absolute values of the MSD's and MSRD's for H:Si(111)-(1×1) and H:C(111)-(1×1) can simply be rationalized by considering the basic differences in phonon bandwidths and bonding strengths of the adatoms to the respective substrates. The onset of classical behavior of all quantities can be rationalized by referring to the properties of appropriate effective one-dimensional oscillators whose characteristic average frequencies depending on layer m and direction α are smaller roughly by a factor of 2 than the respective Debye frequencies. Because of the weaker bonding at and near a surface all MSD's and DCF's are larger than

the corresponding bulk quantities. Thus thermal damping of scattering intensities is always larger at and near a surface than in the bulk. Using isotropic bulk vibronic correlation functions therefore cannot lead to a fully quantitative interpretation of surface-scattering data. Our results demonstrate that the surface dynamical properties of a considered system have to be taken into account for a quantitative calculation of displacement-correlation functions near or at surfaces and we have indicated that a consideration of such quantitative MSD's and DCF's is a necessary prerequisite for a fully quantitative analysis of surface-scattering data. We hope that in the near future such analyses for particular semiconductor surface systems will be carried out in joint theoretical and experimental efforts.

ACKNOWLEDGEMENT

We gratefully acknowledge financial support of this work by the Deutsche Forschungsgemeinschaft (Bonn, Germany) under Contract No. Po 215/8-2.

[1]J. Zegenhagen, Surf. Sci. Rep. **18**, 199 (1993).
[2]R. Feidenhans'l, Surf. Sci. Rep. **10**, 105 (1989).
[3]P. H. Citrin, J. Phys. (Paris) Colloq. **47**, C8-437 (1986); P. A. Lee, P. H. Citrin, P. Eisenberger, and B. M. Kincaid, Rev. Mod. Phys. **53**, 769 (1981).
[4]J. Stöhr, in *X-ray Absorption: Principles, Applications, Techniques of EXAFS, SEXAFS and XANES,* edited by R. Prins and D. Konigsberger (Wiley, New York, 1988).
[5]J. Stöhr, L. Johansson, I. Lindau, and P. Pianetta, Phys. Rev. B **20**, 664 (1979).
[6]J. Stöhr, Condens. Matter **61**, 439 (1985).
[7]S. M. Durbin, L. E. Berman, B. W. Batterman, and J. M. Blakely, J. Vac. Sci. Technol. A **3**, 973 (1985).
[8]M. J. Bedzyk, Q. Shen, M. E. Keeffe, G. Navrotzki, and L. E. Berman, Surf. Sci. **220**, 419 (1989).
[9]G. Dalba, P. Fornasini, G. Giunta, and E. Burattini, J. Non-Cryst. Solids **107**, 261 (1989).
[10]R. E. Martinez, E. Fontes, J. A. Golovchenko, and J. R. Patel, Phys. Rev. Lett. **69**, 1061 (1992).
[11]B. Sandfort, A. Mazur, and J. Pollmann, this issue, Phys. Rev. B **51**, 7139 (1995).
[12]B. Sandfort, A. Mazur, and J. Pollmann, this issue, Phys. Rev. B **51**, 7150 (1995).
[13]Ch. Stuhlmann, G. Bogdányi, and H. Ibach, Phys. Rev. B **45**, 6786 (1992).
[14]P. Dumas and Y. J. Chabal, J. Vac. Sci. Technol. A **10**, 2160 (1992).
[15]A. A. Maradudin, E. W. Montroll, G.H. Weiss, and I. P. Ipatova, *Theory of Lattice Dynamics in the Harmonic Approximation* (Academic, New York, 1971).
[16]A. Mazur and J. Pollmann, Surf. Sci. **225**, 72 (1990).
[17]E. A. Stern, Phys. Rev. B **10**, 3027 (1974).
[18]D. E. Sayers, E. A. Stern, and F. W. Lytle, Phys. Rev. Lett. **27**, 1204 (1971).
[19]G. Beni and P. M. Platzman, Phys. Rev. B **14**, 1514 (1976).
[20]R. McGrath, I. T. McGovern, D. R. Warburton, G. Thornton, and D. Norman, Surf. Sci. **178**, 101 (1986).
[21]R. McGrath, I. T. McGovern, D. R. Warburton, D. Purdie, C. A. Muryn, N. S. Prakash, P. L. Wincott, G. Thornton, D. S.-L. Law, and D. Norman, Phys. Rev. B **45**, 9327 (1992).
[22]P. Roubin, D. Chandesris, G. Rossi, J. Lecante, M. C. Desjonquères, and G. Tréglia, Phys. Rev. Lett. **56**, 1272 (1986).